Journal of Materials Chemistry B

ROYAL SOCIETY OF CHEMISTRY

PAPER

View Article Online
View Journal

Cite this: DOI: 10.1039/d6tb00422a

Hepatocyte purification column using thermoresponsive glycopolymer-modified silica beads

Kenichi Nagase *[ab] and Junnosuke Matsuda[b]

Regenerative medicine involving hepatocytes holds promise as a therapeutic strategy for liver diseases. The clinical application of this approach requires a reliable technique for hepatocyte isolation. In this study, we developed a cell separation column that employs a thermoresponsive glycopolymer to isolate hepatocytes through temperature modulation. Silica beads were coated with poly(*N*-*p*-vinylbenzyl-*O*-β-D-galactopyranosyl-1→4-D-guliconamide)-*b*-poly(*N*-isopropylacrylamide) (PVLA-*b*-PNIPAAm) *via* atom transfer radical polymerization and were used as packing material for the column. The modified beads were characterized using scanning electron microscopy, CHN elemental analysis, Fourier transform infrared spectroscopy, and X-ray photoelectron spectroscopy. Nine columns were fabricated by altering the PNIPAAm and PVLA chain lengths of PVLA-*b*-PNIPAAm. Evaluation of the elution characteristics of HepG2 cells revealed that columns with intermediate PVLA and PNIPAAm chain lengths exhibited temperature-dependent cell retention and elution. This column enabled the separation of HepG2 cells from contaminating RAW264.7 cells by adjusting the temperature. The recovered HepG2 cells retained high levels of activity. Collectively, these findings indicate that the developed column enables efficient separation of hepatocytes solely through temperature modulation.

Received 23rd February 2026,
Accepted 11th May 2026

DOI: 10.1039/d6tb00422a

rsc.li/materials-b

1. Introduction

Over the past few decades, tissue engineering and cell transplantation therapy have emerged as effective strategies for the treatment of challenging diseases.[1–7] Hepatic tissue engineering, in particular, has attracted attention as a promising therapeutic approach for various liver disorders.[8–11] In the field of hepatic tissue engineering, methods for isolating hepatocytes are essential for the successful creation of hepatic tissue, as hepatocytes must be purified from contaminating cells during isolation from liver tissue.

To date, a variety of cell separation techniques have been developed.[12–18] Notably, methods that utilize fluorescently labeled antibodies or magnetic particles are extensively used because they enable precise cell separation. However, these techniques require modification of cell surfaces with fluorescent antibodies or magnetic particles, which can result in the loss of specific cell properties.[19,20] Consequently, there is a demand for cell separation methods that avoid modification of cell surfaces.

To address this issue, we developed a cell separation technique using substrates modified with the thermoresponsive polymer, poly(*N*-isopropylacrylamide) (PNIPAAm).[21–25] PNIPAAm is the most widely used thermoresponsive polymer, characterized by temperature-dependent hydration and dehydration around its phase transition temperature of 32 °C, where it expands upon hydration and contracts upon dehydration.[26–31] This unique thermoresponsive property has been applied in several biomedical fields, including temperature-controlled drug and gene delivery systems,[32–37] biosensors and bioimaging technologies,[38–41] nano-actuators with chemical oscillation,[42–44] temperature-responsive chromatographic analysis using various aqueous mobile phases,[45–55] temperature-modulated bioseparations,[56–64] and cell culture substrates and scaffolds.[65–74] Within the field of cell separation, target cells adhere to the PNIPAAm at 37 °C due to its dehydration and contraction. When the temperature is lowered to 20 °C, PNIPAAm becomes hydrated and expands, causing the attached cells to detach. This temperature-controlled adhesion and detachment facilitate cell separation, as target cells selectively adhere to, or are recovered from, the PNIPAAm-modified substrate.[75] To enhance the selectivity of cell separation, an ionic PNIPAAm copolymer is employed, leveraging the varying

[a] Graduate School of Biomedical and Health Sciences, Hiroshima University, 1-2-3 Kasumi, Minami-ku, Hiroshima City, Hiroshima, 734-8553, Japan. E-mail: nagase@hiroshima-u.ac.jp; Fax: +81-82-257-5323; Tel: +81-82-257-5323
[b] Faculty of Pharmacy, Keio University, 1-5-30 Shibakoen, Minato, Tokyo 105-8512, Japan

ionic properties of cells to enable selective adhesion on PNIPAAm copolymer–modified substrates.[76–81] This method has been found to effectively separate mesenchymal stem cells.[77,78]

On the contrary, poly(*N*-*p*-vinylbenzyl-*O*-β-D-galactopyranosyl-1→4-D-guliconamide) (PVLA), a hepatic affinity polymer, has been developed as a substrate for effective hepatocyte culture, and as a drug delivery carrier targeting hepatocytes.[82–84] PVLA contains galactose moieties that interact with the asialoglycoprotein receptor (ASGPR) of hepatocytes, thereby mediating the affinity between PVLA and hepatocytes. Therefore, PVLA may function as a promising ligand for selective hepatocyte capture in cell separation systems, and PVLA-based separation systems could play a key role in hepatic tissue engineering. Previous studies have achieved selective adhesion and detachment of hepatocytes using glass substrates modified with PVLA and PNIPAAm block copolymers.[85] However, when performing cell separation on polymer-modified glass substrates, the number of cells that can be processed becomes limited. Thus, hepatocyte isolation columns capable of processing large numbers of cells are required.

In this study, we fabricated a temperature-controlled hepatocyte separation column using silica beads modified with PVLA-*b*-PNIPAAm as the packing material. The fabricated column was subsequently evaluated for the temperature-controlled separation of hepatocytes from contaminating cells.

2. Materials and methods

2.1 Fabrication of thermoresponsive glycopolymer-modified beads

Silica beads were coated with a thermoresponsive glycopolymer through immobilization of an atom transfer radical polymerization (ATRP) initiator, followed by a two-step ATRP procedure (Fig. 1).

Silica beads were sorted into two size ranges, 150–180 μm and 180–210 μm, using sieves with mesh sizes of 150 μm and 180 μm. A total of 50.0 g of size-selected silica beads were placed in a 500 mL three-neck round-bottom flask, and 200 mL of hydrochloric acid was added. The mixture was stirred at 90 °C for 3 h. Subsequently, the silica beads were filtered using a membrane filter, washed with ultrapure water, and rinsed with acetone. The cleaned beads were then dried in a vacuum oven at 150 °C for 7 h.

Silanization of the silica beads was carried out as follows. Hydrochloric acid-treated silica beads (10.0 g) were placed in a 500 mL three-neck round-bottom flask. The interior of the flask was humidified to 60% by introducing humidified nitrogen gas, and the beads were maintained at 25 °C for 3 h to achieve humidity. In a glass beaker, dehydrated toluene (300 mL) was mixed with (chloromethyl)phenylethyl-trimethoxysilane (CPTMS) (12.4 mL, 0.05 mol). This mixture was then added to the silica beads in the flask, and the silanization reaction was conducted at 25 °C for 16 h. After completion of the reaction, the silica beads were collected *via* vacuum filtration, rinsed with acetone, and dried at 110 °C for 2 h.

PVLA was grafted onto silica beads using the following method. Initiator-modified silica beads (3.0 g) were placed in a 50 mL glass container. A specific amount of *N*-*p*-vinylbenzyl-*O*-β-D-galactopyranosyl-1→4-D-guliconamide (VLA) was dissolved in a mixed solvent comprising 20 mL water and 20 mL 2-propanol. VLA solutions of 10, 50, and 100 mM were prepared. For instance, in the 10 mmol solution, VLA (189 mg, 0.400 mmol) was dissolved in 40 mL of the mixed solvent. Argon was introduced into the VLA solution while stirring for 20 min to eliminate dissolved oxygen. Subsequently, tris[(2-dimethylamino)ethyl]amine (Me_6TREN) (68.00 mg, 0.30 mmol) and CuCl (26.22 mg, 0.26 mmol) were added, and the flask was sealed. Both the reaction flask and the glass vessel containing the beads were placed in a glove bag, where the air was replaced with argon gas. The reaction mixture was then added to the silica beads in the glass vessel. α-Chloro-*p*-xylene (1.75 μL, 13.2 μmol) was introduced into the solution, and the glass vessel was sealed. ATRP was carried out at 25 °C for 1 h using a shaker for agitation. After the reaction, the bead suspension was centrifuged, and the supernatant was removed. The recovered silica beads, which settled upon centrifugation, were washed with acetone for 30 min under ultrasonic agitation. The beads were then further cleaned using an ultrasonic bath for 30 min in a 1 : 1 mixture of ethylenediamine-*N*,*N*,*N*′,*N*′-tetraacetic acid (EDTA) aqueous solution (50 mM) and methanol. Finally, the beads were filtered, rinsed with water and acetone, and dried in a vacuum oven at 50 °C for 16 h.

The PNIPAAm segment was linked to the PVLA on silica beads *via* a second ATRP step. This procedure was analogous to the initial ATRP step used for VLA polymerization, with the exception that *N*-isopropylacrylamide (NIPAAm) was included in the monomer solution instead, and the reaction time was extended to 16 h. Briefly, a predetermined concentration of NIPAAm was dissolved in 2-propanol. NIPAAm solutions of 500, 1000, and 1500 mM were then prepared. The solution was deoxygenated by bubbling argon gas through it, after which equal amounts of Me_6TREN and CuCl were added. The solution was then allowed to react with PVLA-modified silica beads (3.0 g), and ATRP was carried out at 25 °C for 16 h. After completion of the reaction, the beads were filtered, washed sequentially with acetone and a mixed solvent of 50 mM EDTA aqueous solution and methanol, and then dried in a vacuum oven.

To prepare a comparative column packing material that does not adsorb hepatocytes, silica beads were modified exclusively with PNIPAAm. NIPAAm (4.52 g, 40.0 mmol) was dissolved in 2-propanol (40 mL), and the solution was deoxygenated by bubbling argon gas through it, after which Me_6TREN (68.00 mg, 0.30 mmol) and CuCl (26.22 mg, 0.26 mmol) were added. The reaction mixture was then applied to CPTMS-modified silica beads (3.0 g) in a glass vessel, and ATRP was performed at 25 °C for 16 h. The beads were subsequently washed with acetone and a mixed solvent of EDTA aqueous solution and methanol.

2.2 Characterization of thermoresponsive glycopolymer-modified beads

The polymer-modified silica beads were characterized using CHN elemental analysis, Fourier transform infrared spectroscopy

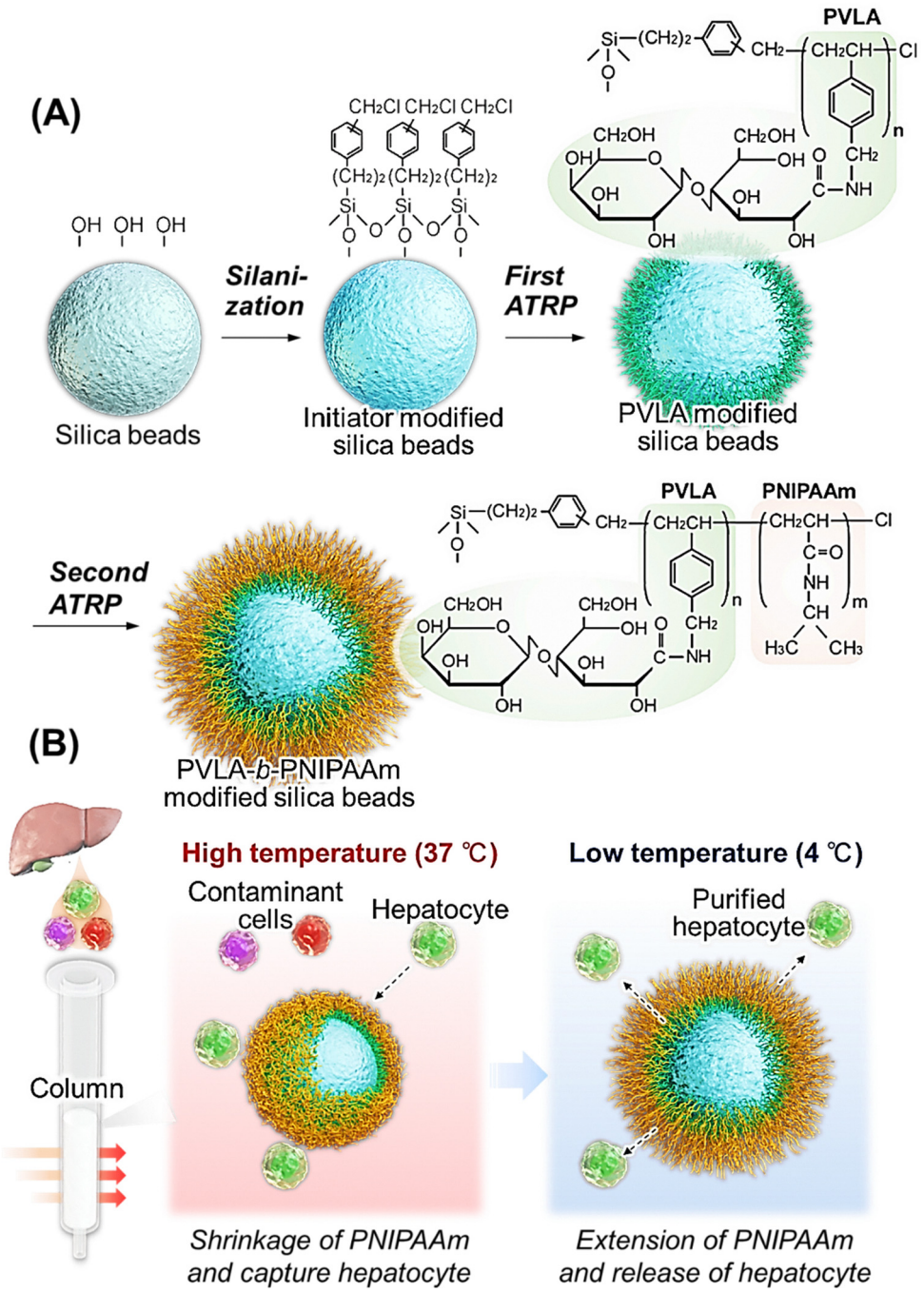

Fig. 1 Schematic illustration of (A) the preparation of PVLA-*b*-PNIPAAm brush–modified silica beads as packing materials *via* tandem ATRP and (B) temperature-modulated capture and release of hepatocytes on the polymer-modified beads within the column. The interaction between PVLA and hepatocytes is mediated by multivalent and dynamic presentation of galactose moieties on flexible polymer side chains, rather than a single-point rigid ligand–receptor binding geometry.

(FT-IR), X-ray photoelectron spectroscopy (XPS), and scanning electron microscopy (SEM).

For elemental analysis, 2.00 mg of initiator-modified and polymer-modified silica beads were weighed and analyzed for carbon, nitrogen, and hydrogen content using an elemental analyzer (Unicube, Elementar, Langenselbold, Germany). The amounts of initiator and polymer modifications were derived from the carbon content using the formula provided in the SI.

The surface elemental composition of the copolymer-modified silica beads was analyzed using XPS (ESCALAB 250; Thermo Fisher Scientific, Waltham, MA, USA). To verify polymer modification of the silica beads, the beads were subjected to FT-IR (FTIR-4700; JASCO, Tokyo, Japan). The morphology of

the copolymer-modified silica beads was examined using SEM (TM4000Plus-II; Hitachi Hightech, Tokyo, Japan).

2.3 Cell elution behavior of the prepared columns

The elution behaviors of HepG2 and RAW264.7 cells from bead-packed columns were evaluated to assess cell separation efficiency. HepG2 cells were used as the target liver cells, whereas RAW264.7 cells served as the contaminant. Each cell type was cultured in a specific medium, as outlined in Table S1 (SI).

RAW264.7 cells (mouse macrophage-like cells) were used as a model non-target cell population, as they do not express the asialoglycoprotein receptor and therefore lack specific affinity for galactose-containing ligands. In addition, macrophage-like cells represent a major class of non-parenchymal cells that may contaminate hepatocyte preparations, making RAW264.7 cells a practical model for evaluating hepatocyte selectivity under flow conditions.

A 50 μm filter was placed at the base of an empty column, and 300 mg of polymer-modified beads were packed into the column. A second 50 μm filter was positioned on top to secure the layer of packed beads. The column was rinsed by passing through a 1 : 1 mixture (100 mL) of methanol and pure water, followed by 100 mL of pure water.

The column was equilibrated by passing 5 mL of William's E medium preheated to 37 °C, through the packed bed. A 1 mL cell suspension containing 5.0×10^5 cells per mL was filtered through a 40 μm cell strainer and then introduced into the column at 37 °C using a syringe pump at a flow rate of 1.0 mL min^{-1}. The effluent collected from the column was designated as ''Load.'' Subsequently, 1 mL of preheated William's E medium (37 °C) was passed through the column at a flow rate of 1.0 mL min^{-1} to flush out non-adsorbed cells while maintaining the column temperature at 37 °C. This step was performed twice, and the resulting effluents were designated as ''Wash''. Both the column and Hank's balanced saline solution (HBSS) with 0.1% EDTA were cooled to 4 °C. HBSS (1 mL) was then passed through the column at a flow rate of 9.0 mL min^{-1} to elute the adsorbed cells. This step was performed thrice, and the collected effluents were designated as ''Elute.'' The cell count in each fraction was determined using an automated cell viability analyzer (Vi-CELL XR; Beckman Coulter, Brea, CA, USA). The elution ratio was calculated by comparing the number of cells eluted to the initial number of cells loaded.

Cell separation experiments were conducted using a similar method, but with a sample containing HepG2 and RAW264.7 cells. RAW264.7 cells were labeled with CellTracker Red (Thermo Fisher Scientific, Waltham, MA, USA), whereas HepG2 cells were left unlabeled. Equal numbers of both cell types were combined, and the resulting cell suspension was introduced into the column at a flow rate of 1 mL min^{-1}. The eluted fraction was collected and designated as ''Load.'' Subsequently, William's E medium was passed through the column at 1.0 mL min^{-1} at 37 °C to remove non-adsorbed cells. This step was repeated four times, and the eluted fraction was collected and designated as ''Wash.'' Next, HBSS with 0.1% EDTA (1 mL) was introduced into the column at 4 °C at a flow rate of 9.0 mL min^{-1} to elute the adsorbed cells. This step was repeated four times, and the eluted fraction was collected and designated as ''Elute.'' The composition of stained and unstained cells in each fraction was determined *via* examination under a fluorescence microscope (BZ-X810; Keyence, Osaka, Japan).

The cell viability of the eluted fractions was determined using a trypan blue exclusion assay with a cell viability analyzer. To assess the growth of the collected HepG2 cells, they were seeded in a 24-well plate (1 mL, 1.0×10^5 cells per mL) and allowed to proliferate for a designated period. Cell numbers were quantified using an automated cell viability analyzer. Control cells, which were not passed through the column, were cultured using the same procedure, and their growth was examined for comparison. Statistical significance was evaluated using Welch's *t*-test and was set at a *P*-value ≤ 0.05.

3. Results and discussion

3.1 Characterization of thermoresponsive glycopolymer-modified beads

Thermoresponsive glycopolymer block copolymer–grafted silica beads were synthesized *via* tandem ATRP. To determine the initiator and polymer content, CHN elemental analysis was conducted on these beads, with a particular focus on carbon composition (Table 1). The grafting amounts were calculated from a CHN elemental analysis conducted according to the equations described in the SI (Section S.2).

Initiator-modified silica beads exhibited a higher carbon content than unmodified ones, indicating successful immobilization of the ATRP initiator CPTMS to the silica beads *via* silanization. The density of immobilized CPTMS was 3.71 μmol m^{-2}, which is comparable to the reported density of surface silanol groups on silica beads.[86] This suggests that most of the silanol groups on the silica beads were used for CPTMS immobilization.

The silica beads grafted with PVLA exhibited a higher carbon content than those immobilized with CPTMS, which is due to the PVLA grafting that occurred during the initial ATRP process. The carbon content increased sequentially from PV10 to PV50, and again from PV50 to PV100, suggesting that longer PVLA chains were attached to the silica beads as the VLA monomer concentration increased during the first ATRP. This is because the polymerization rate of VLA increased with higher monomer concentrations during the ATRP step.87 The rise in carbon content in the PVLA-*b*-PNIPAAm–grafted beads (PV X-PN) was more pronounced than in the PVLA-grafted beads (PV X), owing to the addition of the PNIPAAm segment onto PVLA during the second ATRP.

The copolymer content on the beads varied between 0.176 and 0.421 mg m^{-2}, which is less than previously documented amounts for polymer modification in porous silica beads, used for high-performance liquid chromatography packing materials.[50] This variation is attributed to the difference in the pore size of the silica beads; the pore diameter was 6 nm in

Table 1 Characterization of the prepared thermoresponsive glycopolymer–modified beads

Code[a]	Elemental composition (%)[b]			%$C_{(calcd)}$	Immobilized initiator (μmol m^{-2})[c]	Grafted polymer (mg m^{-2})[c]
	C	H	N			
Non-modified silica beads	0.01	1.18	0.08			
Initiator-immobilized silica beads	14.43	1.897	0.07		3.71	
PV10	15.81	2.23	0.22			0.0748
PV10-PN500	16.34	2.254	0.50			0.176
PV10-PN1000	16.98	2.359	0.68			0.302
PV10-PN1500	17.57	2.443	0.83			0.421
PV50	16.02	2.12	0.20			0.0864
PV50-PN500	17.22	2.24	0.36			0.322
PV50-PN1000	17.25	2.37	0.45			0.328
PV50-PN1500	17.06	2.30	0.52			0.290
PV100	16.78	2.22	0.26			0.131
PV100-PN500	17.16	2.25	0.31			0.205
PV100-PN1000	17.11	2.30	0.41			0.195
PV100-PN1500	17.30	2.24	0.31			0.233
CPTMS				59.5		
NIPAAm				63.7		
VLA				53.3		

[a] The prepared copolymer brush–modified beads are designated as "PV X-PN Y", where X represents the VLA concentration used in the first ATRP step and Y represents the NIPAAm concentration used in the second ATRP step. [b] Elemental composition determined by CHN elemental analysis. [c] Grafted polymer surface density calculated based on carbon composition.

the present study, while it was 30 nm in a previous study.[50] The smaller pore size impeded efficient polymer grafting within the pores of the silica beads, leading to a reduced amount of grafted polymer in the current study.

From the perspective of cell separation, however, the small pore size is advantageous. Because mammalian cells such as HepG2 and RAW264.7 are several orders of magnitude larger than nanometer-scale pores, cell interactions occur exclusively on the external bead surface. The use of small-pore silica beads therefore confines polymer grafting primarily to the bead exterior, ensuring that temperature-dependent cell capture and release are governed by surface-localized polymer brushes rather than polymer chains grown within pore interiors. While non-porous silica beads could also be used in principle for cell separation, the use of small-pore porous beads provides a higher effective surface area for initiator immobilization and more stable polymer brush formation.

XPS analysis was conducted to investigate the surface elemental and carbon bond compositions of the beads (Fig. 2A and Fig. S1, Table S3). Wide-scan and high-resolution XPS spectra are shown in Fig. S1 (SI), and the corresponding elemental compositions are summarized in Table S3. The copolymer-grafted beads showed a surface carbon composition of 34.8%, consistent with previous results on PNIPAAm

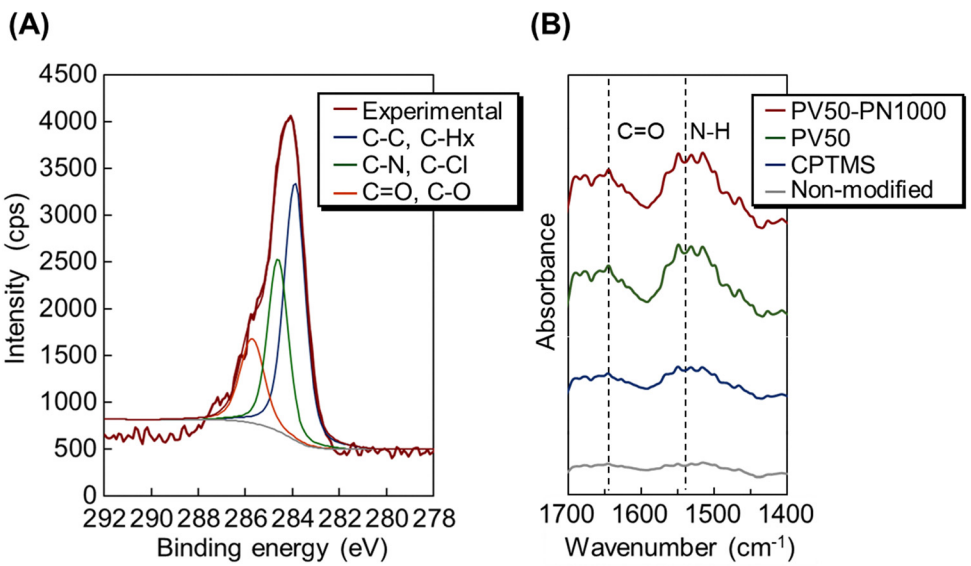

Fig. 2 Characterization of the prepared copolymer-grafted silica beads. (A) X-ray photoelectron spectroscopy spectra of C1s peaks of the PV50-PN1000 beads. (B) FT-IR spectra of the beads. Dashed lines (i) and (ii) represent peaks attributed to the carbonyl groups of the amide bonds.

copolymer brush-grafted silica beads.[88] This indicates that a similar copolymer brush structure was grafted onto the bead surface in this study.

Although the silica beads are made of SiO_2, the detected silicon content was low. These results suggest that the copolymer layer covered the silica beads, effectively masking the detection of silica-based materials. A small amount of chlorine (0.4%) was also detected by elemental analysis, indicating retention of the terminal chlorine atom in the copolymer following the two ATRP reactions.

The sequential ATRP process yields a PNIPAAm-containing polymer brush layer on the bead surface, which is primarily formed through chain extension of PVLA termini, however, the possible coexistence of a minor fraction of PNIPAAm homopolymer brushes cannot be completely excluded in surface-initiated systems.

The copolymer brush exhibited C1s peaks, including an additional peak at a binding energy of approximately 288 eV corresponding to carbonyl groups (Fig. 2A). These findings confirm the successful modification of the copolymer through ATRP.

FT-IR analysis (Fig. 2B) confirmed the polymer modifications during both the initial and subsequent ATRP reactions. In the PVLA-grafted beads (PV50) and the PVLA-*b*-PNIPAAm-grafted beads (PV50-PN1000), peaks were observed at 1550 and 1650 cm^{-1}, corresponding to the amide bonds present in the polymers on the beads. In contrast, these peaks were absent in unmodified beads, confirming successful copolymer grafting onto the silica beads through ATRP.

The morphology of the beads following each reaction was analyzed using SEM (Fig. 3). The silica beads retained their original morphology and size, with no evidence of deformation or aggregation. This finding indicates that the sequence of reactions for silane coupling and ATRP did not affect the structure of the silica beads. A previous study reported that excessive grafting of PNIPAAm onto silica beads caused agglomeration.[89] However, our block copolymer brush–grafted silica beads exhibited a smooth surface. This result implies that the two ATRPs produced a consistent polymer coating.

3.2 Cell elution behavior of the prepared columns

The prepared beads were loaded into columns to examine the elution behavior of HepG2. To determine the optimal bead diameter for column packing, PNIPAAm-modified beads with two different diameters were used: 150–180 μm and 180–210 μm (Fig. 4). PNIPAAm-modified beads were selected as packing materials because a previous study showed that PNIPAAm does not effectively adsorb hepatocytes, even at elevated temperatures.[85] Consequently, cells pass through the column without adhering to the packing material, enabling assessment of the influence of the particle size of the packing material on cell movement. Columns packed with 150–180 μm beads resulted in minimal cell recovery. Conversely, columns packed with 180–210 μm beads exhibited notable cell elution in the Load fraction. This occurs because larger beads create bigger gaps between them, facilitating cell passage. In contrast, smaller beads result in tighter spaces, hindering cell movement and causing them to become trapped. Based on these findings, beads with a diameter of 180–210 μm were selected as the optimal packing material for columns.

To verify the interaction between PVLA and hepatocytes, silica beads modified exclusively with PVLA (PV10) were prepared and placed into a column. PV10 was used in this experiment to examine whether ASGPR-mediated hepatocyte

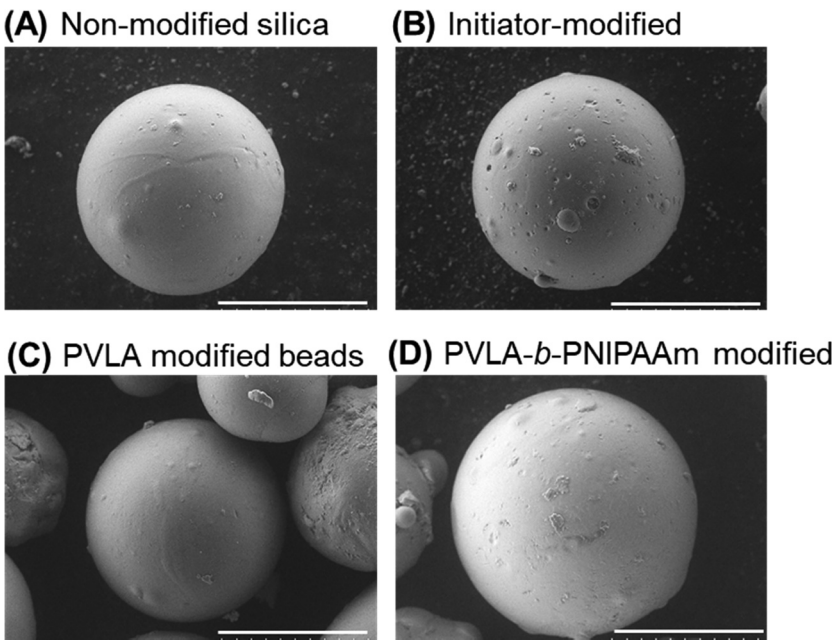

Fig. 3 SEM image of the prepared polymer-modified silica beads. Scale bar, 100 μm. (A) Non-modified silica beads, (B) Initiator (CPTMS)-modified silica beads, (C) PVLA modified silica beads (PV10), (D) PVLA-*b*-PNIPAAm modified silica beads (PV10-PN1500).

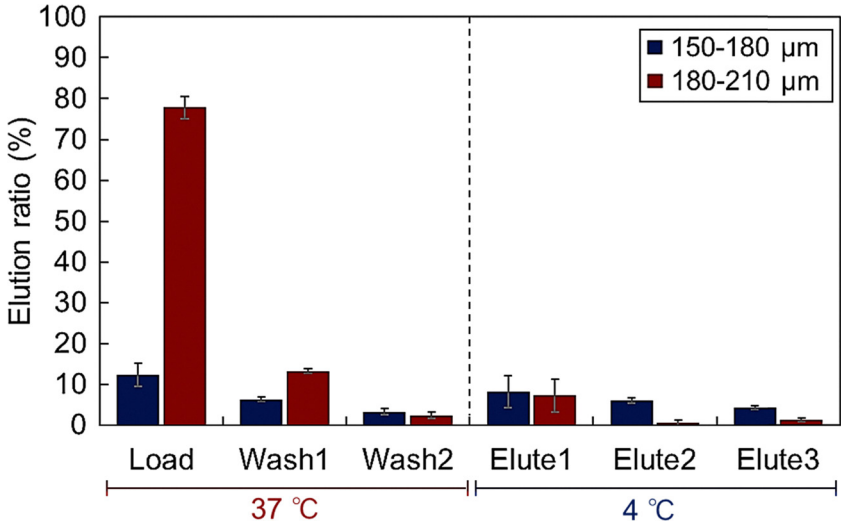

Fig. 4 Elution behavior of HepG2 cells from a PNIPAAm-modified bead-packed column using beads of various diameters.

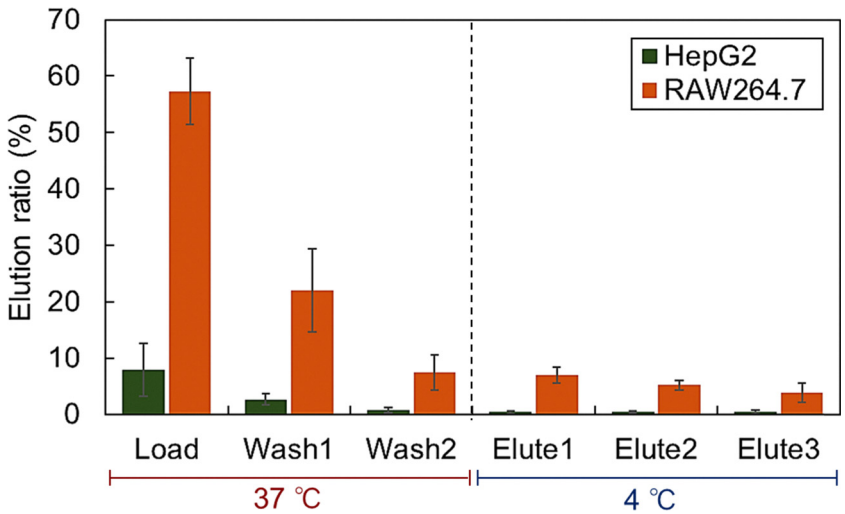

Fig. 5 Elution behavior of HepG2 and RAW264.7 cells from a PVLA-modified bead-packed column (PV10), evaluating the affinity between PVLA and HepG2 cells.

interaction can be detected even at a low PVLA grafting density, providing sensitive conditions for evaluating the presence of specific cell–polymer interactions. HepG2 and RAW264.7 cells were introduced into the column, and their elution profiles were analyzed (Fig. 5). HepG2 cells exhibited minimal elution from the column at both 37 °C and 4 °C, due to their strong interaction with PVLA within the column. Conversely, most RAW264.7 cells eluted in the first fraction, indicating a weak interaction with PVLA. These findings demonstrate that PVLA can effectively interact with HepG2 as it flows through the column.

Although the presence of a polymer backbone may introduce steric constraints, the strong retention of HepG2 cells on PVLA-modified beads (Fig. 5), together with the negligible interaction observed for RAW264.7 cells, demonstrates that sufficient fractions of galactose moieties remain accessible to ASGPR under flow conditions. These results provide experimental evidence that polymer architecture does not preclude functional receptor recognition, but rather enables effective hepatocyte capture through collective and flexible ligand presentation.

Next, HepG2 elution behavior was evaluated using columns packed with PVLA-*b*-PNIPAAm-modified silica beads (Fig. 6). To examine the effect of PNIPAAm chain length in PVLA-*b*-PNIPAAm, packing materials were prepared with a fixed PVLA length of 10 mM (PV10) and varying PNIPAAm lengths of 500 mM (PV10-PN500), 1000 mM (PV10-PN1000), and 1500 mM (PV10-PN1500). Compared to columns containing only PVLA, those packed with PVLA-*b*-PNIPAAm-modified beads exhibited a greater tendency for elution of HepG2 cells. This occurs

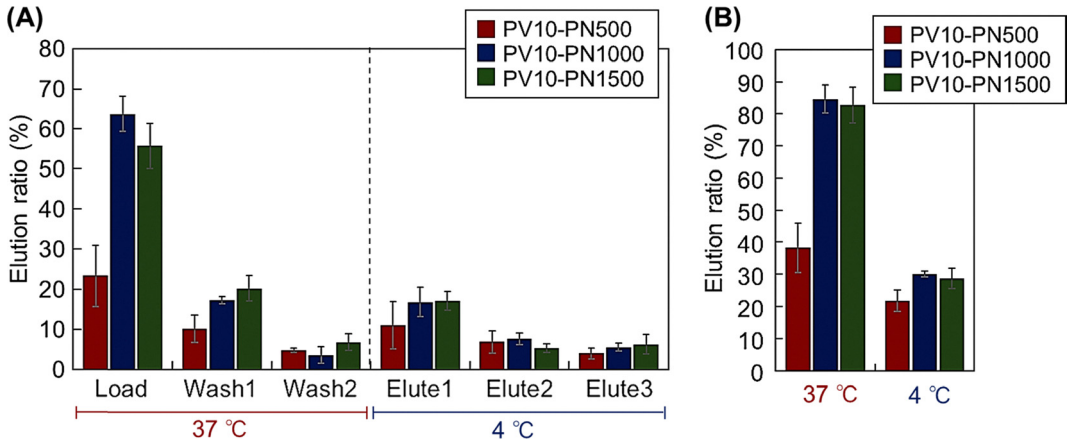

Fig. 6 Elution behavior of HepG2 cells from a PVLA-*b*-PNIPAAm-modified bead-packed column with varying PNIPAAm lengths. (A) Elution ratio at each fraction, and (B) elution ratio at 37 °C and 4 °C.

because PNIPAAm conceals PVLA, thereby reducing the interaction between PVLA and HepG2 cells. For PV10-PN500, which possesses a short PNIPAAm chain length, the HepG2 elution ratio in the 37 °C load and wash fractions was low. This is attributable to the shorter PNIPAAm chain length, facilitating easier access for HepG2 to the underlying PVLA layer. Conversely, for PV10-PN1000 and PV10-PN1500, the HepG2 elution ratio in the 37 °C load and wash fractions was high. This is because the PNIPAAm chains in these bead formulations were long enough to hinder HepG2 cells from reaching the basal PVLA layer. Consequently, a greater proportion of HepG2 cells was eluted in the load and wash fractions using PV10-PN1000 and PV10-PN1500. By lowering the temperature to 4 °C, a small proportion of adsorbed HepG2 cells was eluted from the column. At low temperatures, the PNIPAAm segment becomes hydrated and extended. Hydration and extension of the PNIPAAm segment physically mask and spatially separate PVLA from the cell surface, thereby diminishing effective multivalent interactions with ASGPR. As a result, previously adsorbed HepG2 cells are released without chemical disruption of ligand–receptor binding. The elution ratios of HepG2 cells for PV10-PN1000 and PV10-PN1500 were slightly higher than that for PV-PN500. This is because the short PNIPAAm segment was insufficient to reduce HepG2 affinity, even in the extended state caused by hydration. Therefore, a certain length of PNIPAAm is required to elute HepG2 cells from the column upon temperature change.

Taken together, these results indicate that the accessibility of PVLA is governed not solely by the fraction of block formation, but by the overall surface coverage and spatial organization of the PNIPAAm-containing polymer brush layer.

Furthermore, to examine the effect of PVLA chain length in PVLA-*b*-PNIPAAm, packing materials were prepared with a fixed PNIPAAm length of 1000 mM (PN1000) and varying PVLA lengths of 10 mM (PV10-PN100), 50 mM (PV50-PN1000), and 100 mM (PV100-PN1000) (Fig. 7). As the PVLA chain length increased, the elution ratio of HepG2 at 37 °C decreased, reflecting the stronger interaction between HepG2 and PVLA as the PVLA chain length becomes longer. Conversely, at 4 °C, almost no HepG2 cells were eluted from PV100-PN1000,

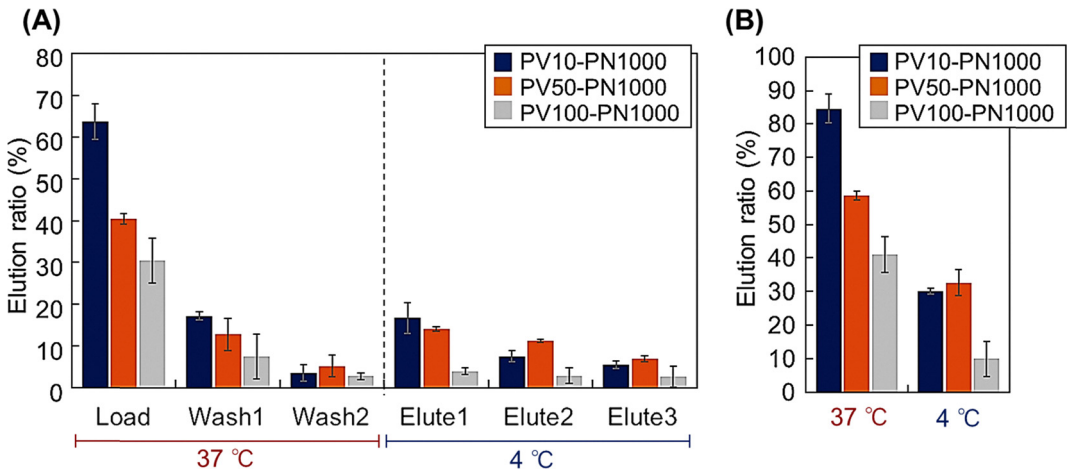

Fig. 7 Elution behavior of HepG2 cells from a PVLA-*b*-PNIPAAm-modified bead-packed column with varying PVLA lengths. (A) Elution ratio at each fraction, and (B) elution ratio at 37 °C and 4 °C.

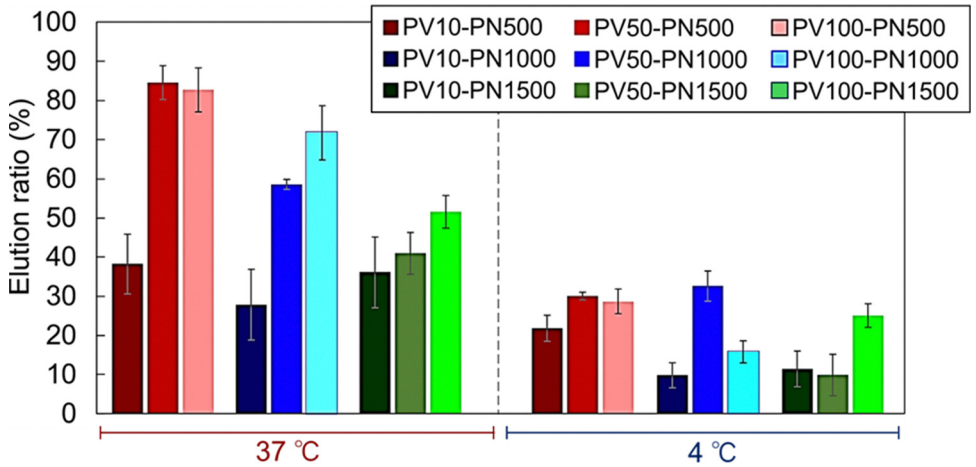

Fig. 8 Comparison of HepG2 elution ratios from nine columns packed with silica beads grafted with varying PVLA and PNIPAAm lengths.

suggesting that the interaction between HepG2 cells and PVLA became excessively strong when the PVLA chain length was increased. These findings suggest that a long PVLA segment in PVLA-*b*-PNIPAAm is not ideal for temperature-controlled elution of HepG2 cells.

The elution ratios of HepG2 cells at 37 °C and 4 °C were evaluated using nine columns packed with silica beads coated with varying lengths of PVLA and PNIPAAm (Fig. 8). Comparison using the nine columns showed that longer PNIPAAm chains generally reduced HepG2 retention at 37 °C whereas longer PVLA chains appeared to enhance HepG2 retention at the same temperature. However, at 4 °C, the PV50-PN1000 column exhibited a relatively high elution ratio compared with the other columns. This suggests that PV50-PN1000 possesses PVLA and PNIPAAm chains of optimal lengths, enabling the effective elution of HepG2 cells adsorbed onto PVLA by extending the PNIPAAm chains. Consequently, PV50-PN1000 was determined to be the most efficient among the nine column types.

RAW264.7 cells, which served as a reference cell line, were applied to PV50-PN1000 to compare their elution behavior with that of HepG2 cells (Fig. 9). Most RAW264.7 cells were eluted at 37 °C due to their lack of ASGPR expression and affinity with PVLA. Conversely, at 4 °C, nearly all RAW264.7 cells remained uneluted, as most had already eluted at 37 °C. In contrast, HepG2 cells, which adhered to the column, began to elute as the temperature dropped. These findings suggest that by loading both cell lines onto the column at 37 °C and subsequently reducing the temperature, a high concentration of HepG2 cells may be obtained.

To assess the effectiveness of the column in cell separation, a mixture of HepG2 and RAW264.7 cells in equal proportions were applied to the column, and their elution patterns were analyzed (Fig. 10). In the mixed-cell experiments, the elution ratio was not separately quantified because the entire eluted suspension was used for microscopic analysis to determine the cell composition ratio.

During the load and wash steps at 37 °C, a significant number of RAW264.7 cells were detected in the eluted fractions. In contrast, during the Elute step at 4 °C, a large number of HepG2 cells were collected in the eluted fractions. These findings demonstrate that the developed column effectively isolates hepatocytes from other contaminating cells.

In our previous study, hepatocyte separation was demonstrated using a thermoresponsive glycopolymer-modified glass substrate.[85] While effective selective adhesion and detachment were achieved, the number of cells that could be processed in a single separation experiment was inherently limited by the planar geometry and available surface area of the substrate.

Compared with our previously reported glass substrate–based separation system, the present bead-packed column enables approximately five-fold higher cell processing capacity per separation cycle, highlighting its advantage in throughput and scalability rather than direct numerical comparison of recovery or purity under differing experimental conditions.

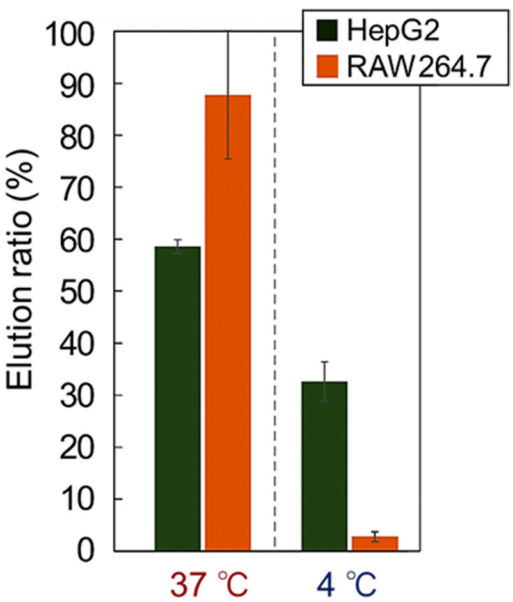

Fig. 9 Comparison of elution behavior between HepG2 and RAW264.7 cells from a PV50-PN1000-modified bead-packed column.

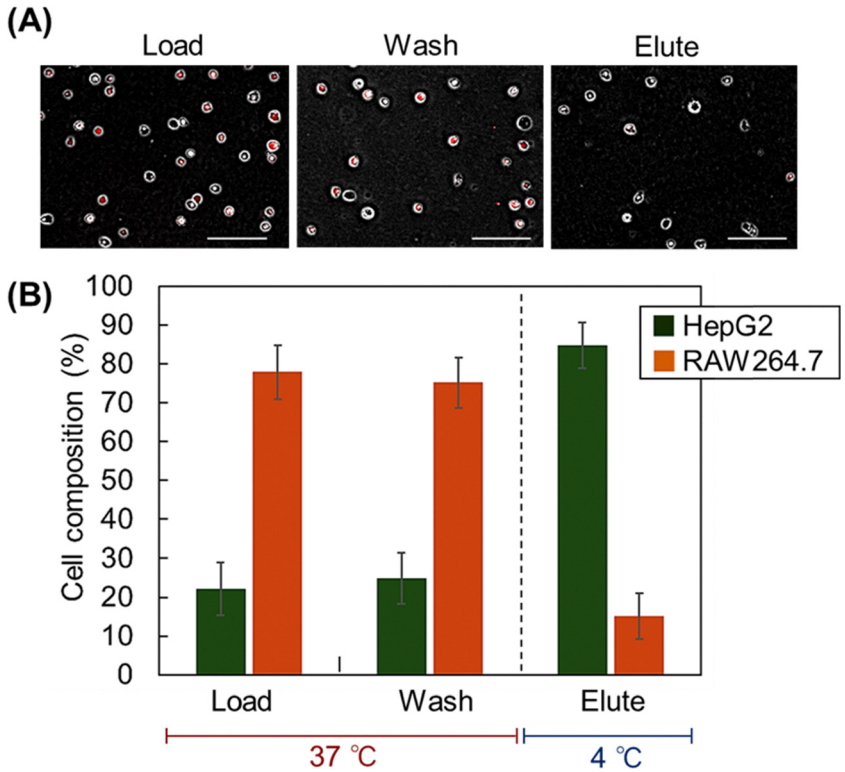

Fig. 10 Separation of a mixed population of HepG2 and RAW264.7 cells using a PV50-PN1000 column. (A) Fluorescence images of cell suspensions in each fraction. HepG2 cells were unstained, and RAW264.7 cells were stained red. Scale bar, 100 μm. (B) Cell composition in each fraction.

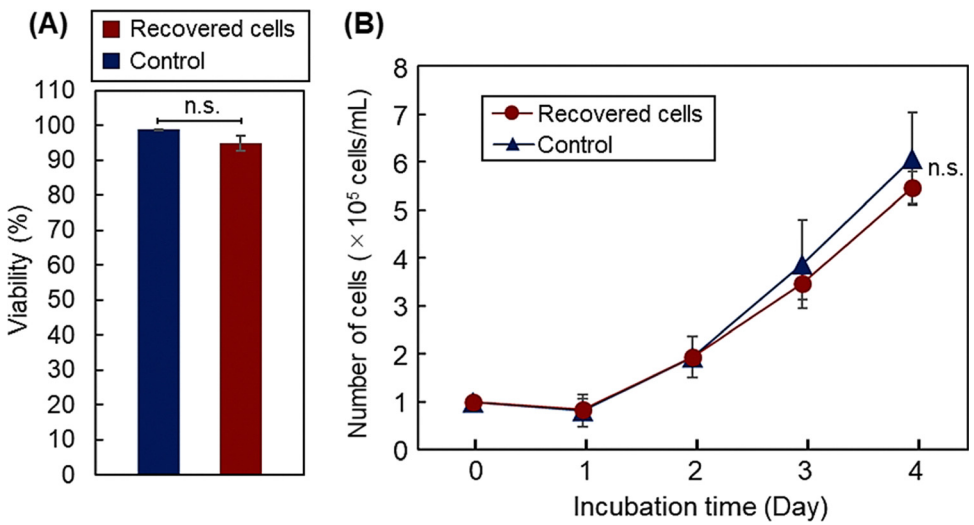

Fig. 11 Cell activity of cells recovered from the PV50-PN1000 column. ''Control'' indicates cells that were not subjected to column loading. (A) Cell viability determined by trypan blue exclusion assay. (B) Proliferation curves of the recovered cells. ''n.s.'' indicates not significant.

To determine whether the cell separation process impaired cell activity, we compared the survival rate and proliferative capacity of cells before and after passage through the column (Fig. 11). HepG2 cell viability was assessed using the trypan blue exclusion assay (Fig. 11A). HepG2 cells that were eluted from the column exhibited viability comparable to that of control cells that were not passed through the column, suggesting that the constructed cell separation column does not affect cell viability. Furthermore, we evaluated HepG2 cell proliferation (Fig. 11B). The results indicated that the proliferative behavior of HepG2 cells eluted from the column was comparable to that of control cells that were not passed through the

column, suggesting that the column does not influence cell proliferation.

Collectively, these findings indicate that the cell separation column fabricated with a thermoresponsive glycopolymer efficiently separates hepatocytes from non-target cells by exploiting a temperature-sensitive interaction between the polymers and hepatocytes. This method preserves the cells' functionality and keeps the cell surface intact. Thus, this column could serve as a valuable tool for cell therapy and tissue engineering applications involving hepatocytes.

4. Conclusions

We developed a column packed with silica beads that were modified using block copolymers composed of thermoresponsive polymers and glycopolymers. The PVLA-*b*-PNIPAAm was attached to the silica beads through silanization and ATRP. Alteration of the monomer concentration during ATRP enabled adjustment of the segment lengths of PVLA and PNIPAAm. Elemental analysis, XPS, and FT-IR were used to evaluate the polymer-modified silica beads, confirming the successful modification of the copolymer. After determining the appropriate particle size of silica beads that HepG2 cells can traverse, it was established that a size range of 180–210 μm is optimal. A column packed with beads modified only with PVLA retained HepG2 cells but allowed RAW264.7 cells to elute, reflecting the interaction between PVLA and HepG2. Increasing the PNIPAAm segment length in PVLA-*b*-PNIPAAm reduced HepG2 cell retention at elevated temperatures and enhanced its elution at lower temperatures, as the interaction between PVLA and HepG2 diminishes with longer PNIPAAm segments. Conversely, increasing the PVLA segment length improved HepG2 retention at high temperatures and reduced its release at low temperatures, as longer PVLA segments strengthen the interaction with HepG2. Consequently, columns with balanced PVLA and PNIPAAm chain lengths, specifically PV50-PN1000, enabled effective retention and elution of HepG2 cells under temperature regulation. This column enabled the separation of HepG2 cells from contaminating cells through controlled temperature regulation. The HepG2 cells recovered from the column retained their activity, indicating that the column represents a valuable tool for cell therapy and tissue engineering applications involving hepatocytes.

Conflicts of interest

There are no conflicts of interest.

Data availability

Data are available from the corresponding author upon reasonable request.

Supplementary Information (SI), including detailed materials, calculation methods for grafting amounts, cell culture conditions, and characterization data (XPS spectra and elemental analysis), is available. See DOI: https://doi.org/10.1039/d6tb00422a.

Acknowledgements

This study received funding from a Grant-in-Aid for Scientific Research (grant nos. JP21KK0199, JP22K19899, JP24K01181 and JP25K22918) and JSPS Program for Forming Japan's Peak Research Universities (J-PEAKS) grant number JPJS00420230011 provided by the Japan Society for the Promotion of Science. In addition to this, research grants were also provided by the Precise Measurement Technology Promotion Foundation (PMTP-F), the CASIO Science Promotion Foundation, and the Mukai Science and Technology Foundation. The work was conducted with the facilities in the Core Facility Management Center at Hiroshima University with assistance of Prof. Hiroki Miyaoka and Mr. Reiji Sunamoto.

References

1 R. Langer and J. Vacanti, *Science*, 1993, **260**, 920–926.
2 P. Menasché, A. A. Hagège, M. Scorsin, B. Pouzet, M. Desnos, D. Duboc, K. Schwartz, J.-T. Vilquin and J.-P. Marolleau, *Lancet*, 2001, **357**, 279–280.
3 T. Shin'oka, Y. Imai and Y. Ikada, *N. Engl. J. Med.*, 2001, **344**, 532–533.
4 K. Nishida, M. Yamato, Y. Hayashida, K. Watanabe, N. Maeda, H. Watanabe, K. Yamamoto, S. Nagai, A. Kikuchi, Y. Tano and T. Okano, *Transplantation*, 2004, **77**, 379–385.
5 T. Iwata, M. Yamato, K. Washio, T. Yoshida, Y. Tsumanuma, A. Yamada, S. Onizuka, Y. Izumi, T. Ando, T. Okano and I. Ishikawa, *Regener. Ther.*, 2018, **9**, 38–44.
6 M. Sato, M. Yamato, G. Mitani, T. Takagaki, K. Hamahashi, Y. Nakamura, M. Ishihara, R. Matoba, H. Kobayashi, T. Okano, J. Mochida and M. Watanabe, *npj Regener. Med.*, 2019, **4**, 4.
7 K. Yamamoto, M. Yamato, T. Morino, H. Sugiyama, R. Takagi, Y. Yaguchi, T. Okano and H. Kojima, *npj Regener. Med.*, 2017, **2**, 6.
8 K. M. Kulig and J. P. Vacanti, *Transplant Immunology*, 2004, **12**, 303–310.
9 Y. Nahmias, F. Berthiaume and M. L. Yarmush, in *Tissue Engineering II: Basics of Tissue Engineering and Tissue Applications*, ed. K. Lee and D. Kaplan, Springer Berlin Heidelberg, Berlin, Heidelberg, 2007, pp. 309–329, DOI: 10.1007/10_029.
10 K. Matsuura, R. Utoh, K. Nagase and T. Okano, *J. Control. Release*, 2014, **190**, 228–239.
11 T. Takebe, K. Sekine, M. Enomura, H. Koike, M. Kimura, T. Ogaeri, R.-R. Zhang, Y. Ueno, Y.-W. Zheng, N. Koike, S. Aoyama, Y. Adachi and H. Taniguchi, *Nature*, 2013, **499**, 481–484.
12 J. C. Giddings, N. Barman Bhajendra and M.-K. Liu, in *Cell Separation Science and Technology*, American Chemical Society, Washington DC, 1991, vol. 464, ch. 9, pp. 128–144.

13 R. K. Kumar and A. W. J. Lykke, *Pathology*, 1984, **16**, 53–62.
14 K. Kataoka, Y. Sakurai, T. Hanai, A. Maruyama and T. Tsuruta, *Biomaterials*, 1988, **9**, 218–224.
15 M. Kamihira and A. Kumar, in *Advances in Biochemical Engineering/Biotechnology*, ed. A. Kumar, I. Galaev and B. Mattiasson, Springer, Berlin/Heidelberg, 2007, vol. 106, pp. 173–193.
16 A. Mahara and T. Yamaoka, *Biomaterials*, 2010, **31**, 4231–4237.
17 M. Yamada, W. Seko, T. Yanai, K. Ninomiya and M. Seki, *Lab on a Chip*, 2017, **17**, 304–314.
18 A. Otaka, K. Kitagawa, T. Nakaoki, M. Hirata, K. Fukazawa, K. Ishihara, A. Mahara and T. Yamaoka, *Langmuir*, 2017, **33**, 1576–1582.
19 L. A. Herzenberg, D. Parks, B. Sahaf, O. Perez, M. Roederer and L. A. Herzenberg, *Clinical Chemistry*, 2002, **48**, 1819–1827.
20 S. Miltenyi, W. Müller, W. Weichel and A. Radbruch, *Cytometry*, 1990, **11**, 231–238.
21 K. Nagase, N. Mukae, A. Kikuchi and T. Okano, *Macromol. Biosci.*, 2012, **12**, 333–340.
22 K. Nagase, R. Shukuwa, T. Onuma, M. Yamato, N. Takeda and T. Okano, *J. Mater. Chem. B*, 2017, **5**, 5924–5930.
23 K. Nagase, R. Shukuwa, H. Takahashi, N. Takeda and T. Okano, *J. Mater. Chem. B*, 2020, **8**, 6017–6026.
24 K. Nagase, Y. Sakurada, S. Onizuka, T. Iwata, M. Yamato, N. Takeda and T. Okano, *Acta Biomater.*, 2017, **53**, 81–92.
25 K. Nagase, M. Shimura, R. Shimane, K. Hanaya, S. Yamada, A. M. Akimoto, T. Sugai and H. Kanazawa, *Biomaterials Science*, 2021, **9**, 663–674.
26 M. Heskins and J. E. Guillet, *J. Macromol. Sci., Part A: Pure Appl. Chem.*, 1968, **2**, 1441–1455.
27 A. Halperin, M. Kröger and F. M. Winnik, *Angew. Chem., Int. Ed.*, 2015, **54**, 15342–15367.
28 K. Nagase, T. Onuma, M. Yamato, N. Takeda and T. Okano, *Macromol. Rapid Commun.*, 2015, **36**, 1965–1970.
29 K. Nagase, J. Matsuda, A. Takeuchi and Y. Ikemoto, *Surf. Interfaces*, 2023, **40**, 103058.
30 K. Nagase, K. Yamaoka, R. Shimane, N. Kojima, N. L. Yamada, H. Seto and Y. Fujii, *Surf. Interfaces*, 2024, **54**, 105268.
31 K. Nagase, T. Ikarashi, H. Zhang, N. Kojima, T. Fukuma and K. Miyata, *Mater. Today Chem.*, 2025, **49**, 103041.
32 M. Nakayama, J. Akimoto and T. Okano, *J. Drug Targeting*, 2014, **22**, 584–599.
33 M. K. Jaiswal, M. Gogoi, H. Dev Sarma, R. Banerjee and D. Bahadur, *Biomater. Sci.*, 2014, **2**, 370–380.
34 D. D. Nguyen, L.-J. Luo and J.-Y. Lai, *Materials Today Bio*, 2022, **13**, 100183.
35 K. Nagase, M. Hasegawa, E. Ayano, Y. Maitani and H. Kanazawa, *Int. J. Mol. Sci.*, 2019, **20**, 430.
36 R. Nemoto, K. Fujieda, Y. Hiruta, M. Hishida, E. Ayano, Y. Maitani, K. Nagase and H. Kanazawa, *Colloids Surf., B*, 2019, **176**, 309–316.
37 M. Maekawa-Matsuura, K. Fujieda, Y. Maekawa, T. Nishimura, K. Nagase and H. Kanazawa, *ACS Omega*, 2019, **4**, 6443–6451.
38 T. Mori and M. Maeda, *Langmuir*, 2004, **20**, 313–319.
39 M. Ebara, J. M. Hoffman, A. S. Hoffman and P. S. Stayton, *Lab on a Chip*, 2006, **6**, 843–848.
40 J. M. Hoffman, P. S. Stayton, A. S. Hoffman and J. J. Lai, *Bioconjugate Chem.*, 2015, **26**, 29–38.
41 M. Matsuura, M. Ohshima, Y. Hiruta, T. Nishimura, K. Nagase and H. Kanazawa, *Int. J. Mol. Sci.*, 2018, **19**, 1646.
42 R. Yoshida, *Polym. J.*, 2022, **54**, 827–849.
43 T. Masuda, A. M. Akimoto, M. Furusawa, R. Tamate, K. Nagase, T. Okano and R. Yoshida, *Langmuir*, 2018, **34**, 1673–1680.
44 K. Homma, T. Masuda, A. M. Akimoto, K. Nagase, K. Itoga, T. Okano and R. Yoshida, *Small*, 2017, **13**, 1700041.
45 K. Nagase and H. Kanazawa, *Anal. Chim. Acta*, 2020, **1138**, 191–212.
46 K. Nagase, S. Kitazawa, S. Yamada, A. M. Akimoto and H. Kanazawa, *Anal. Chim. Acta*, 2020, **1095**, 1–13.
47 K. Nagase, M. Watanabe, F. Zen and H. Kanazawa, *Anal. Chim. Acta*, 2019, **1079**, 220–229.
48 K. Nagase, K. Matsumoto and H. Kanazawa, *Sci. Rep.*, 2022, **12**, 4434.
49 K. Nagase, J. Kobayashi, A. Kikuchi, Y. Akiyama, H. Kanazawa and T. Okano, *ACS Appl. Mater. Interfaces*, 2013, **5**, 1442–1452.
50 K. Nagase, A. Mizutani Akimoto, J. Kobayashi, A. Kikuchi, Y. Akiyama, H. Kanazawa and T. Okano, *J. Chromatogr. A*, 2011, **1218**, 8617–8628.
51 A. Mizutani, K. Nagase, A. Kikuchi, H. Kanazawa, Y. Akiyama, J. Kobayashi, M. Annaka and T. Okano, *J. Chromatogr. B*, 2010, **878**, 2191–2198.
52 K. Nagase, J. Kobayashi, A. Kikuchi, Y. Akiyama, H. Kanazawa, M. Annaka and T. Okano, *Biomacromolecules*, 2010, **11**, 215–223.
53 Y. Hiruta, *Chromatography*, 2025, **46**, 11–18.
54 K. Nagase, *Anal. Sci.*, 2024, **40**, 827–841.
55 Y. Maekawa, N. Okamoto, Y. Okada, K. Nagase and H. Kanazawa, *Sci. Rep.*, 2020, **10**, 8828.
56 K. Nagase, M. Geven, S. Kimura, J. Kobayashi, A. Kikuchi, Y. Akiyama, D. W. Grijpma, H. Kanazawa and T. Okano, *Biomacromolecules*, 2014, **15**, 1031–1043.
57 K. Nagase, J. Kobayashi, A. Kikuchi, Y. Akiyama, H. Kanazawa and T. Okano, *RSC Advances*, 2016, **6**, 93169–93179.
58 K. Nagase, S. Ishii, A. Takeuchi and H. Kanazawa, *Sep. Purif. Technol.*, 2022, **299**, 121750.
59 K. Nagase, S. Kitazawa, T. Kogure, S. Yamada, K. Katayama and H. Kanazawa, *Sep. Purif. Technol.*, 2022, **286**, 120445.
60 K. Nagase, K. Yamazaki, Y. Maekawa and H. Kanazawa, *Materials Today Bio*, 2023, **18**, 100521.
61 D. Nomoto, K. Nagase, Y. Nakamura, H. Kanazawa, D. Citterio and Y. Hiruta, *Colloids Surf., B*, 2021, **205**, 111890.
62 Y. Maekawa, K. Yamazaki, M. Ihara, K. Nagase and H. Kanazawa, *Anal. Bioanal. Chem.*, 2020, **412**, 5341–5351.
63 K. Nagase and H. Kanazawa, *Anal. Sci.*, 2025, **41**, 1251–1267.
64 K. Nagase, *Polym. J.*, 2026, **58**, 181–205.
65 N. Yamada, T. Okano, H. Sakai, F. Karikusa, Y. Sawasaki and Y. Sakurai, *Makromol. Chem., Rapid Commun.*, 1990, **11**, 571–576.

66 Y. Akiyama, A. Kikuchi, M. Yamato and T. Okano, *Langmuir*, 2004, **20**, 5506–5511.
67 H. Takahashi, M. Nakayama, M. Yamato and T. Okano, *Biomacromolecules*, 2010, **11**, 1991–1999.
68 H. M. El-Husseiny, E. A. Mady, L. Hamabe, A. Abugomaa, K. Shimada, T. Yoshida, T. Tanaka, A. Yokoi, M. Elbadawy and R. Tanaka, *Mater. Today Bio*, 2022, **13**, 100186.
69 K. Nagase, M. Nagaoka, J. Matsuda and N. Kojima, *Mater. Design*, 2024, **239**, 112824.
70 K. Nagase, M. Watanabe, A. Kikuchi and T. Okano, *Biomater. Sci.*, 2025, **13**, 1657–1670.
71 M. Nakao, M. Matsui, K. Kim, N. Nishiyama, D. W. Grainger, T. Okano, H. Kanazawa and K. Nagase, *Stem Cell Res. Ther.*, 2023, **14**, 352.
72 K. Nagase, H. Kuramochi and H. Takahashi, *Biol. Pharm. Bull.*, 2025, **48**, 1107–1110.
73 M. Nakao and K. Nagase, *Regener. Ther.*, 2024, **26**, 80–88.
74 K. Nagase, H. Kuramochi, D. W. Grainger and H. Takahashi, *Mater. Today Bio*, 2025, **32**, 101657.
75 K. Nagase, A. Kimura, T. Shimizu, K. Matsuura, M. Yamato, N. Takeda and T. Okano, *J. Mater. Chem.*, 2012, **22**, 19514–19522.
76 K. Nagase, N. Uchikawa, T. Hirotani, A. M. Akimoto and H. Kanazawa, *Colloids Surf., B*, 2020, **185**, 110565.
77 K. Nagase, G. Edatsune, Y. Nagata, J. Matsuda, D. Ichikawa, S. Yamada, Y. Hattori and H. Kanazawa, *Biomater. Sci.*, 2021, **9**, 7054–7064.
78 K. Nagase, A. Ota, T. Hirotani, S. Yamada, A. M. Akimoto and H. Kanazawa, *Macromol. Rapid Commun.*, 2020, **41**, 2000308.
79 T. Hirotani and K. Nagase, *Regener. Ther.*, 2024, **27**, 259–267.
80 K. Nagase, A. Okada, J. Matsuda, D. Ichikawa, Y. Hattori and H. Kanazawa, *Colloids Surf., B*, 2022, **220**, 112928.
81 K. Nagase, D. Inanaga, D. Ichikawa, A. Mizutani Akimoto, Y. Hattori and H. Kanazawa, *Colloids Surf., B*, 2019, **178**, 253–262.
82 A. Kobayashi, T. Akaike, K. Kobayashi and H. Sumitomo, *Makromol. Chem., Rapid Commun.*, 1986, **7**, 645–650.
83 M. Goto, H. Yura, C.-W. Chang, A. Kobayashi, T. Shinoda, A. Maeda, S. Kojima, K. Kobayashi and T. Akaike, *J. Control. Release*, 1994, **28**, 223–233.
84 S.-H. Kim, T. Hoshiba and T. Akaike, *Biomaterials*, 2004, **25**, 1813–1823.
85 K. Nagase, N. Kojima, M. Goto, T. Akaike and H. Kanazawa, *J. Mater. Chem. B*, 2022, **10**, 8629–8641.
86 R. F. de Farias and C. Airoldi, *J. Therm. Anal. Calorim.*, 1998, **53**, 751–756.
87 D. Xiao and M. J. Wirth, *Macromolecules*, 2002, **35**, 2919–2925.
88 K. Nagase, J. Kobayashi, A. Kikuchi, Y. Akiyama, H. Kanazawa and T. Okano, *RSC Advances*, 2015, **5**, 66155–66167.
89 K. Nagase, J. Kobayashi, A. Kikuchi, Y. Akiyama, H. Kanazawa and T. Okano, *Langmuir*, 2007, **23**, 9409–9415.